Front. Earth Sci. 2022, 16(3): 587–600
https://doi.org/10.1007/s11707-021-0945-2

RESEARCH ARTICLE

Role of bedding planes played in enhancing dissolution in sandstones

Jin LAI (✉)[1,2], Xiaojiao PANG[2], Meng BAO[2], Bing WANG[2], Jianan YIN[2], Guiwen WANG (✉)[1,2], Xuechun FAN[2]

1 State Key Laboratory of Petroleum Resources and Prospecting, China University of Petroleum (Beijing), Beijing 102249, China
2 College of Geosciences, China University of Petroleum (Beijing), Beijing 102249, China

© Higher Education Press 2021

Abstract Diagenesis exerts an important control on porosity evolution, and research of diagenesis and diagenetic minerals provides insights into reservoir quality evaluation and CO_2 storage. Thin section, XRD (X-ray diffraction), CT (Computed Tomography), scanning electron microscopy (SEM), and NMR (Nuclear Magnetic Resonance) tests were used to investigate composition, texture, pore spaces, and diagenesis of sandstones in Paleogene Dongying Formation in Bohai Bay Basin, China, with special aims to unravel diagentic dissolution along bedding planes. The oversized pores, remnants in feldspar-hosted pores, and kaolinite within feldspar grains indicate a high degree of dissolution the framework grains experienced during burial. The CO_2-rich or organic acids are responsible for the feldspar dissolution. Grain size plays the primary role in enhancing bedding dissolution process, and bedding planes in fine-medium grained sandstones with high content of feldspars are frequently enlarged by dissolution. The CT scanning image confirms dissolution pores are distributed discontinuously along the bedding planes. The dissolution pores along bedding planes have large pore size, and correspond to the right peak of the bi-modal T_2 (transverse relaxation time) spectrum. The laminated sandstones and siltstones, or sandstones with cross beddings help improve framework grain dissolution. These new findings help improve the understanding of diagenetic models, and have implications in reservoir quality prediction and resource assessments in sandstones.

Keywords dissolution, sandstones, diagenesis, bedding plane, Dongying Formation

Received April 5, 2021; accepted August 24, 2021

E-mails: laijin@cup.edu.cn (Jin LAI),
wanggw@cup.edu.cn (Guiwen Wang)

1 Introduction

Diagenesis exerts a strong control on reservoir quality and heterogeneity in sandstones (de Segonzac, 1968; Stonecipher et al., 1984; Al-ramadan et al., 2005; Higgs et al., 2007; Morad et al., 2010; Lai et al., 2017; Bjørlykke, 2014; Liu et al., 2015; Garzanti, 2019; Jafari et al., 2020; Wang et al., 2021). Framework grain dissolution is a natural consequence of diagenesis due to increasing burial depth and temperature (Taylor et al., 2010; Lai et al., 2015). As an important diagenetic modification, dissolution can occur at shallow burial conditions due to meteoric water fluxing, and at deep burial environments because of organic acid-rich or CO_2-rich fluids (Rossi et al., 2001; Islam, 2009; Chen et al., 2017; Lai et al., 2020). Dissolution of framework grains significantly enhances porosity in sandstone (Bowen et al., 2011). Additionally, these secondary dissolution pores are hardly decreased by subsequent compaction (Henares et al., 2016; Saïag et al., 2016; Yue et al., 2018; Lai et al., 2020).

Cross-laminations are internal sedimentary structures in sedimentary rocks, and they are important for sedimentological interpretation (Tucker, 2003; Xu et al., 2015). The bedding planes in layered rocks are weak interfaces, and they are the main factors contributing to the branching of fractures (Flewelling et al., 2013; Chang et al., 2015; Lee et al., 2015; Tang et al., 2018; Weng et al., 2018). The sedimentary beddings can affect fracture growth and act as pathways for fluid flow especially when they are intersected by fractures (Chang et al., 2015; de Silva et al., 2016; Swanson, 2007; Zhou et al., 2018; Momeni et al., 2019). In fine-grained rocks, the lamina (beddings) are favorable for the formation of bedding parallel fractures, and they play important roles in hydrocarbon storage capacity and pore structure (Huang et al., 2018; Liu et al., 2019). The diagenetic changes at the lamina scale are important for hydrocarbon migration and accumulation (Liang et al., 2018). Diagenetic dissolution can make

bedding planes more visible in outcrops (Bathurst, 1987), indicating the phenomenon of bedding enhanced dissolution. However, previous investigations into diagenetic enhancement of beddings have been restricted in lithologies in terms of lime mudstone/marl alternations (Bathurst, 1987), micrite (Feng et al., 2013), and salt/dolostone interfaces (Zhang et al., 2019). Among them, the calcareous and gypsum minerals are dissolved along the weak bedding planes (Bathurst, 1987; Feng et al., 2013; de Silva et al., 2016; Zhang et al., 2019), and bedding dissolution only occurred on layer interfaces within a limestone-siltstone or siltstone-salt interfaces (Feng et al., 2013; Zhang et al., 2019). Fractures can enhance frame work dissolution (Lai et al., 2021). However, whether the diagenetic dissolution in sandstones can occur along the layer structures (bedding planes) remains an open research question.

In this study, special attention is paid to whether the presences of weak bedding interfaces (bedding planes) can improve grain dissolution in the Paleogene Dongying Formation in Nanpu Sag, Bohai Bay Basin, China. Cores are described in terms of lithology, grain size and beddings (laminations and cross beddings). Thin sections, XRD (X-ray diffraction) and SEM (scanning electron microscopy) images are observed to unravel the composition, diagenesis, diagenetic minerals, beddings and pore systems distributed along the bedding interfaces. Then micro-CT (Computed Tomography) scanning is used to provide insights into the bedding dissolution pores. Additionally the pore size distribution of bedding dissolution pores is described using NMR tests, and effect of dissolution pores on the immobility of pore systems is unraveled. The question whether diagenetic dissolution in sandstones can occur along bedding planes is answered from thin section, CT and NMR analysis. The results will provide scientific guidance in the diagenesis model of sandstones, and have practical implications in reservoir quality evaluation and resource assessments. In addition, the insights into the diagenetic modification within lamina scales will provide guidance for shale oil exploration and development in fine-grained sedimentary rocks, in which the lamina are well developed (Huang et al., 2018; Liu and Liu, 2019; Liu et al., 2019).

2 Geologic settings

The Bohai Bay Basin (area of 20×10^4 km^2) is a Cenozoic rift basin, and it appears as a northeast-trending N-shaped geometry (Dong et al., 2010; Guo et al., 2016). The petroliferous Nanpu Sag is located at northeast Huanghua Depression within Bohai Bay Basin (Fig. 1) (Chen et al., 2016; Guo et al., 2016; Lai et al., 2020). The Nanpu Sag is a half-graben basin (Guo et al., 2013). The Cenozoic sedimentary successions consist of Eocene Kongdian (E_k), Eocene Shahejie (E_s), Paleogene Dongying (E_d), Neogene Guantao (N_g), Minghuazhen (N_m) and Quaternary Pingyuan (Q_p) Formation in an ascending order (Chen et al., 2016; Jiang et al., 2016; Zhang et al., 2017; Niu et al., 2020).

The depositional facies of Dongying Formation is interpreted as fan-braided delta (Dong et al., 2015; Liu et al., 2017; Lai et al., 2020). The thick lacustrine mudstones and black shales of the third Member of Shahejie Formation (E_{d_3}) and the third Member of Dongying Formation (E_{s_3}) are organic matter-rich source rocks (Xu et al., 2006; Guo et al., 2013; Lai et al., 2019). The Member 1 of Dongying Formation (E_{d_1}) is the principal reservoir rocks (Dong et al., 2015). The traps are dominantly structural traps or structure-related lithologic traps, and faults are the main hydrocarbon migration pathways (Guo et al., 2013).

3 Samples and methods

A total of 30 thin sections were cut perpendicular to cross beddings, and were analyzed using the Leica optical microscope at the State Key Laboratory of Petroleum Resources and Prospecting. Thin sections were impregnated with resin (blue) for pore system observation and stained with Alizarin red S and K-ferricyanide carbonate mineral identification.

Scanning electron microscopy (SEM) measurements were conducted on 8 gold coated, freshly broken plugs, and the FEI Quanta 200 was used to identify the micropores (< 10 μm) as well as clay minerals (Table 1).

Thirty samples were used for X-ray diffraction (XRD) analysis, which was performed on whole-rock and clay fractions (< 2 μm) to obtain the mineral content (clay minerals, quartz, feldspar, and carbonate, etc). The various minerals were identified from the diffractograms through referencing to the ICDD Powder Diffraction File (Yandoka et al., 2015).

Eight core plug samples (1 inch in diameter) were scanned using a μCT (micro-CT) instrument. The CT scanning provides two-dimensional (2D) images, and generates 3D grayscale images by overlapping 2D grayscale CT images (Cnudde and Boone, 2013; Zhang et al., 2020).

NMR T_2 spectrum was measured using a CoreSpec-1000 NMR instrument with a magnetic field frequency of 2M HZ on the eight samples. The movable water was removed using a centrifugal machine, and the T_2 distributions at saturated and centrifuged status were measured, respectively. The waiting time (T_w) and echo-time (T_e) are set as 6000 ms and 0.2 ms (Lai et al., 2018, 2019; Wang et al., 2020).

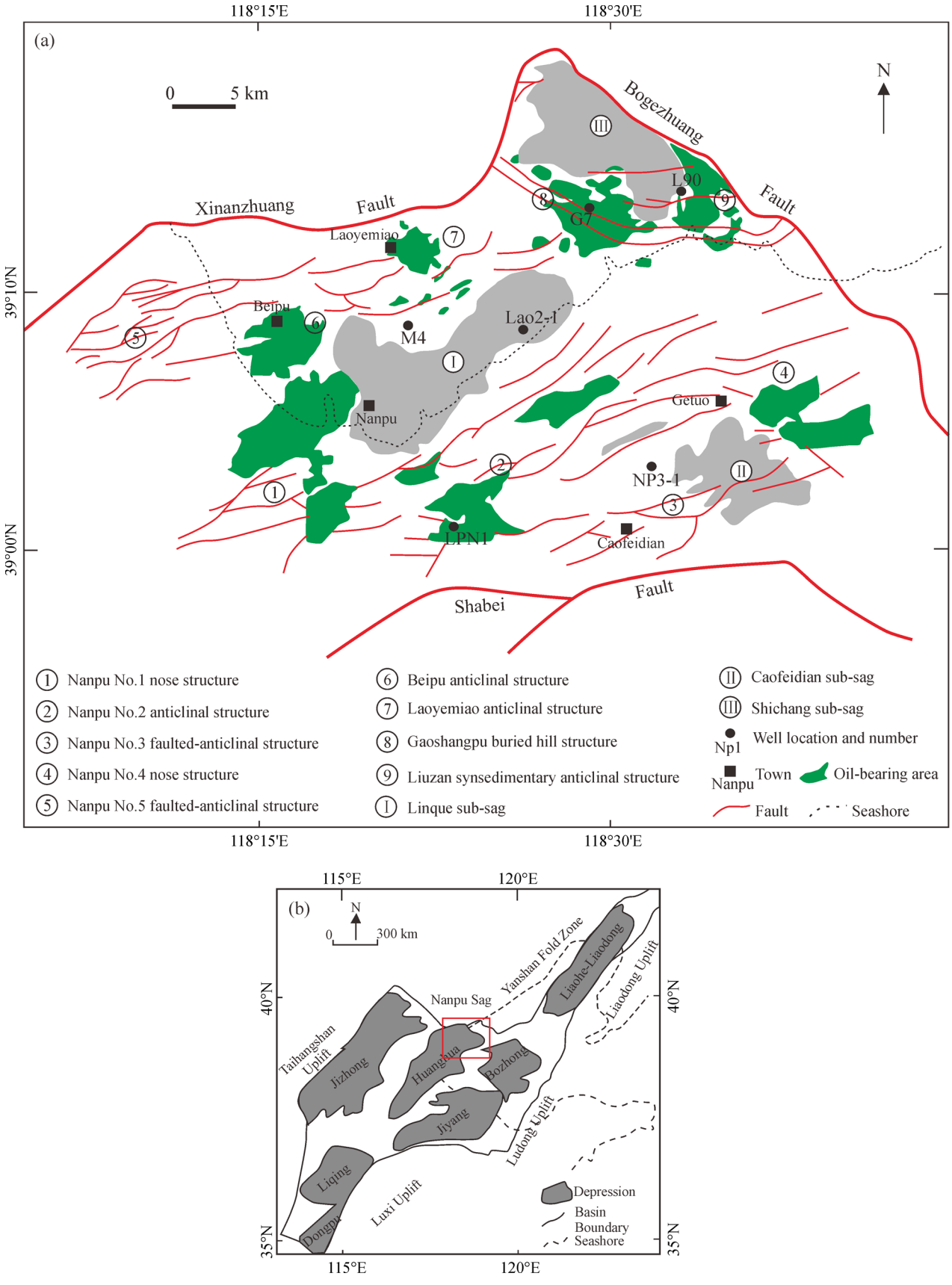

Fig. 1 (a) The structural belts of Nanpu Sag within (b) Bohai Bay Basin (Guo et al., 2013; Lai et al., 2019).

Table 1 The samples used for various measurements

Sample	Well	Depth/m	Thin section	SEM	NMR	CT
1	NP11-E4-X508	2778.15	√	√	√	√
2	NP11-E4-X508	2781.58	√	√	√	√
3	NP13-1274	3219.83	√	√	√	√
4	NP13-1508	3482.07	√	√	√	√
5	NP23-2630	3170.58	√	√	√	√
6	NP23-X2282	3138.2	√	√	√	√
7	NP208	2394.8	√	√	√	√
8	NP208	2534.08	√	√	√	√

4 Results

4.1 Lithology and pore spaces

The lithology of Paleogene Dongying Formation (burial depths 2500–4500 m) is dominantly fine-medium grained sandstone, and siltstone interbedded with gray-black mudstone (Fig. 2). Parallel bedding, cross beddings (tabular and wedge-shape), convolute beddings as well as wavy beddings are observed (Fig. 2). As for the mineral composition, the sandstones consists of 42 wt.%–4 wt.% quartz, 18 wt.%–44 wt.% feldspar, 9 wt.%–34 wt.% clay minerals, and 0 wt.%–15.8 wt.% carbonate minerals according to XRD analysis.

The porosity of Paleogene Dongying sandstones ranges from 1.7% to 32.3% and the permeability is in the range from 0.001 mD to 1819 mD (averaged as 108.7 mD). Thin section shows that pore spaces of the sandstones in Dongying Formation contain a combination of primary intergranular pores (Figs. 3(a) and 3(b)), and secondary pores due to dissolution (partly to complete) of framework grains (mainly feldspars) (Figs. 3(c) and 3(d)). Micropores coexist with clay minerals (mainly authigenic vermicular kaolinite and webby illite/smectite mixed layers) (Figs. 3(e) and 3(f)).

4.2 Diagenesis and diagenetic minerals

As observed by thin section analysis, the dominance of point and point-long grain contacts and abundance of primary pores indicate sandstones in the Dongying Formation had only experienced moderate degree of mechanical compactions (Figs. 3(a)–3(d)). Extensive compaction will significantly reduce porosity (Zhang et al., 2021). The dominant diagenetic minerals include abundant carbonates, various clay minerals and minor amounts of quartz (Guo et al., 2013; Chen et al., 2017; Lai et al., 2019, 2020). However, the framework grains are generally intensively dissolved, which can be evidenced by dominance of secondary dissolution pores (Figs. 3(c) and 3(d)). Thin sections also indicate that the authigenic kaolinites are commonly coexisting with feldspar-hosted dissolution pores (Lai et al., 2018) (Figs. 3(c) and 3(d)). Additionally, SEM observations confirm that abundant feldspars are dissolved, and there are some feldspar remnants or even kaolinites within the partly dissolved feldspar dissolution pores (Figs. 3(g) and 3(h)). The feldspar grains can be dissolved in the early diagenetic stage due to meteoric water flushing, and during burial stages due to organic acids after hydrocarbon charge (Chen et al., 2017). Framework grain dissolution is pervasive in the sandstones (Fig. 3) (Chen et al., 2017; Lai et al., 2019, 2020).

5 Discussion

5.1 Insights from thin section and CT analysis

Cross beddings or laminations are commonly observed in cores, and the bedding planes are frequently enlarged by late burial dissolution, especially in those fine-medium grained sandstones with laminations and cross beddings (Figs. 2(a)–2(e)). However, in some siltstones or very fine grained sandstones which are also abundant in cross beddings (wavy or convolute), no evident dissolution along bedding planes are detected (Figs. 2(f)–2(g)). Therefore grain size may play the primary role in controlling diagenetic dissolution process along the bedding planes (Fig. 2). Thin section petrography and XRD analysis confirm that these sedimentary beddings/laminations are mainly feldspar grains or rock fragments or even clay minerals (Fig. 4). The dissolution rate of feldspars is much higher than that of quartz at certain burial environments (Worthington et al., 2016). The laminated sandstones or sandstones with cross beddings have a relatively higher content of clay as well as feldspar content compared with the massive sandstones by XRD analysis (Figs. 4(a)–4(c)). Presumably, the laminated sandstones or sandstones with cross-beddings originally contain more feldspars than are now present sine some of the preexisting feldspars are dissolved (Fig. 3). Laminations/beddings are

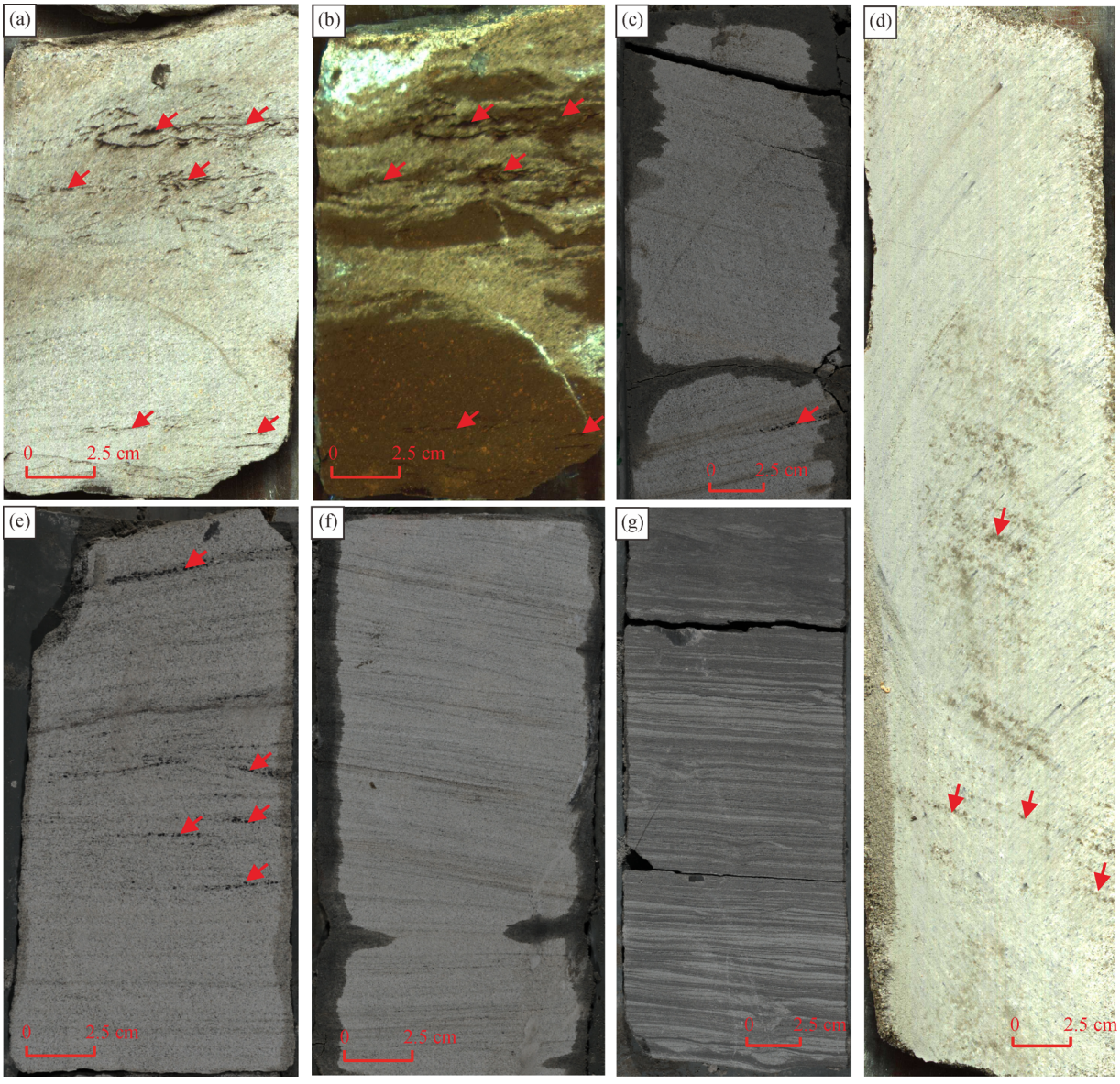

Fig. 2 Core photos showing the cross bedding of sandstones in Dongying Formation in Nanpu Sag. (a) Dissolution along the bedding plane, fine-medium grained sandstone, NP 23-2630; (b) field view A under ultraviolet (UV) light; (c) dissolution along the tabular cross bedding, fine-medium grained sandstone, X204; (d) dissolution along the wedge-shape cross bedding, fine grained sandstone, NP 23-2630; (e) dissolution along the parallel bedding, fine-medium grained sandstone, X204; (f) no evident dissolution occurred along the parallel bedding plane, siltstone, X204; (g) no evident dissolution occurred along the wavy and convolute bedding planes, siltstone, X204.

commonly associated with fine-medium grained sandstones, in which dissolution pores are aligned along bedding planes (Figs. 4(a)–4(b)). Crude oil/bitumen commonly invaded into the bedding planes (Fig. 4(b)). Conversely, the massive (no beddings) sandstones have high quartz content but low feldspar and clay content, which can be evidenced by the thin section observation (Figs. 4(d)–4(f)).

Fractures (diagenetic in origin) are easily to be formed parallel to beddings due to changed rock properties and *in situ* stress associated with bedding interfaces (Zeng and Li, 2009; Chang et al., 2015). Additionally, diagenetic fractures can further improve the grain dissolution along fracture planes (Zazoun, 2013; Anders et al., 2014; Dashti et al., 2018).

Here in this study, it is confirmed that the sedimentary beddings in sandstones can also enhance dissolution along the bedding interfaces. The 2D slices indicate the presences of laminations in the fine-grained sandstones (Fig. 5(a)). The extraction of pores reveals that several

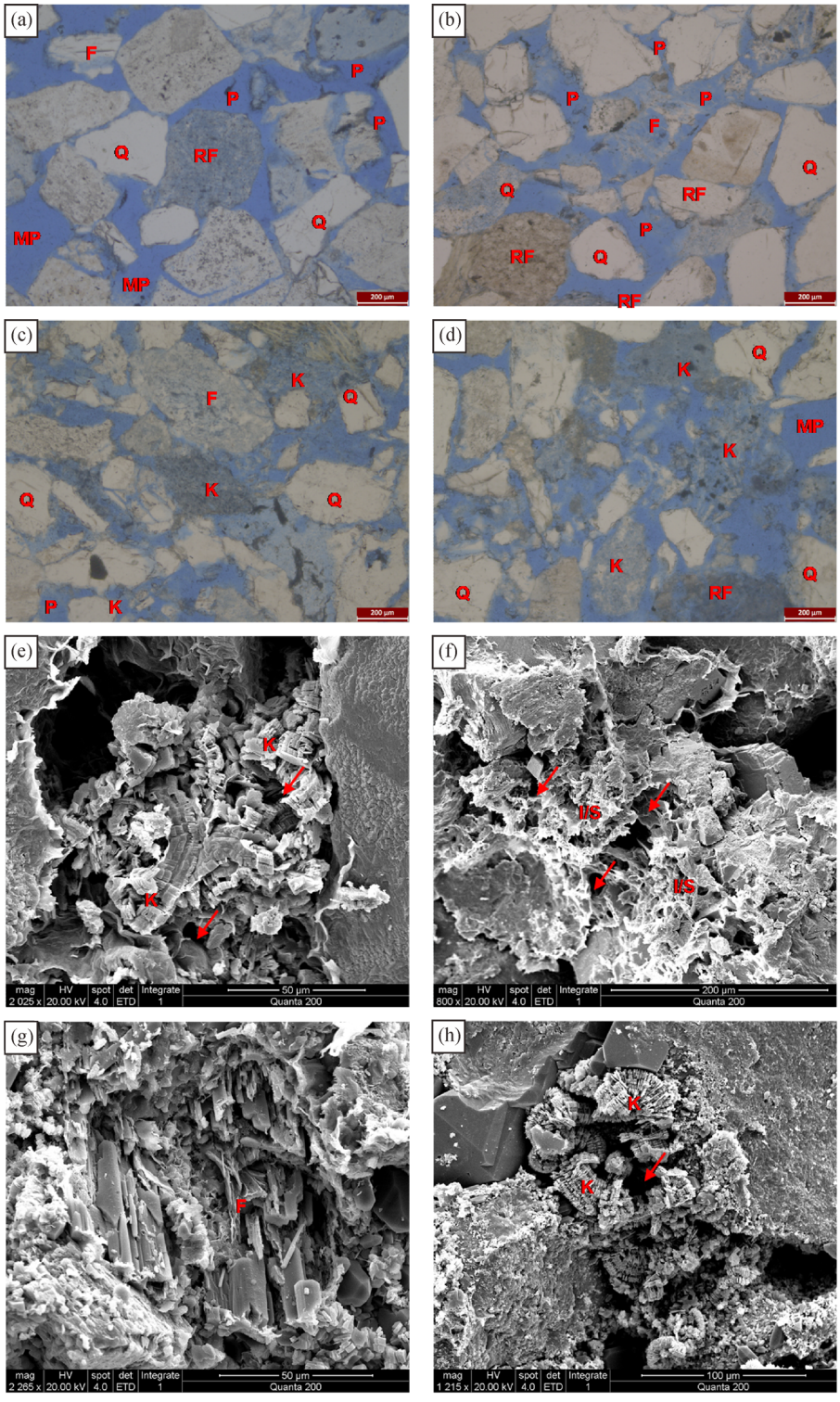

Fig. 3 Pore spaces of the sandstones in Dongying Formation, Nanpu Sag. (a) Intergranular pores and dissolution pores, PPL; (b) primary pores and abundant dissolution pores, PPL; (c) primary intergranular pores and abundant dissolution pores, NP208; (d) abundant intragranular dissolution pores, and minor intergranular pores, NP208; (e) micro-porous kaolinites, SEM; (f) micro-porous mixed layer illite/smectite, SEM; (g) feldspar remnants in the dissolution pores, SEM; (h) vermicular kaolinites within the feldspar-hosted dissolution pores, SEM. PPL = plane polarized light view; I/S = mixed layer illite/smectite; K = Kaolinite; P = Pores; MP = Moldic pores; Q = quartz; RF = rock fragments; F = Feldspar.

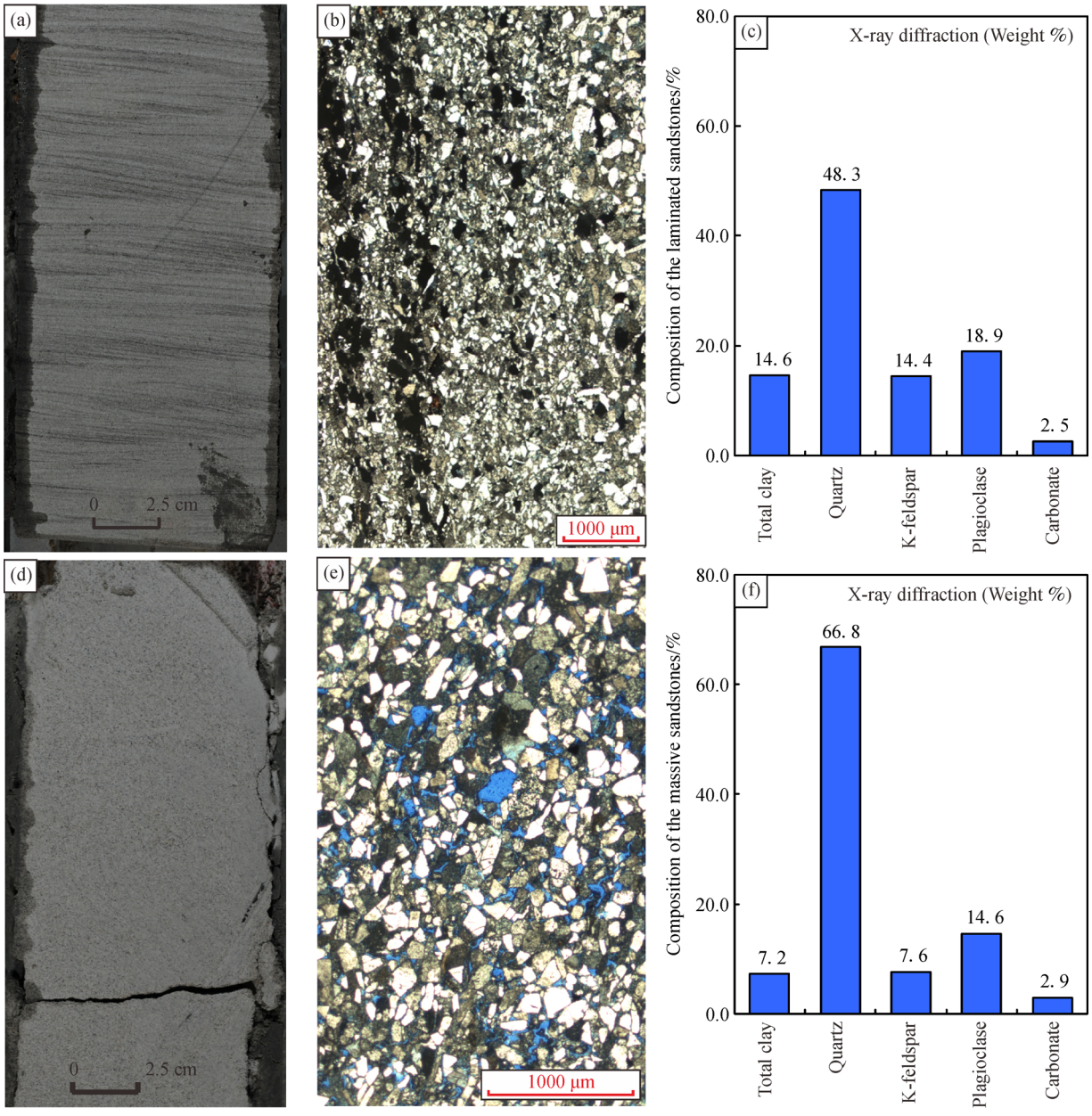

Fig. 4 Contrast of laminated sandstones with massive sandstones (no bedding) through core, thin section and XRD analysis. (a) Laminated sandstones; (b) thin section showing the laminas, NP23-X2284, 3150.6m; (c) XRD data showing the composition of the laminated sandstones; (d) massive sandstones; (e) related thin section image showing the pore spaces and composition of massive sandstone; (f) XRD data showing the composition of the massive sandstones.

aligned pore system layers are observed, and the (dissolution) pores are distributed discontinuously along the bedding planes (Fig. 5(b)). In addition, the 3D reconstruction of pore networks confirms the bedding planes with traces of dissolution, and the pore size of dissolution pores range from tens of micrometers to 200–300 μm (Fig. 5(c)). The microscopic thin section photomicrographs confirm the presences of aligned dissolution pores (100–300 μm in pore sizes) along the bedding planes (Fig. 5(d)). The dissolved framework grains are mainly feldspars, forming partly dissolution pores or even moldic pores (Fig. 5(d)). The white quartz grains have a directional alignment (Fig. 5(d)).

The more evident in bedding interfaces, the more dissolution pores are observed. For instance, the bedding planes are obviously observed by 2D CT image (Fig. 6(a)), and the 3D reconstruction of pore networks show abundant dissolution pores (200–300 μm in pore sizes) are obviously

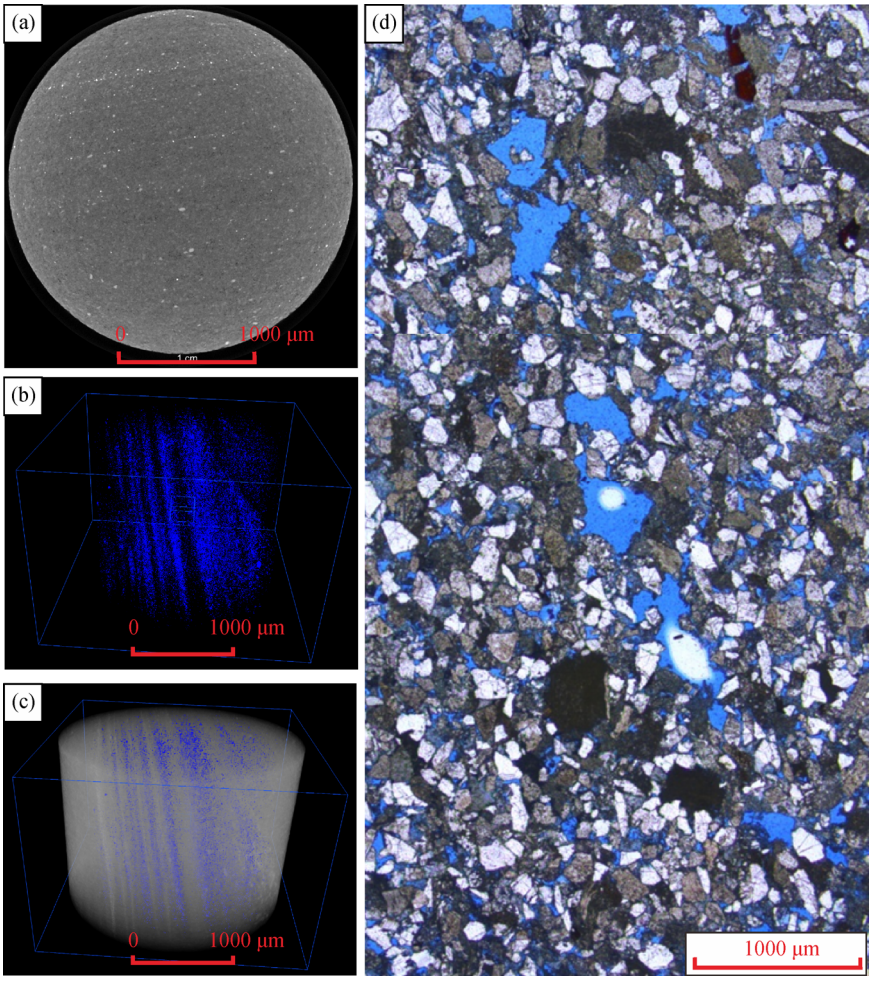

Fig. 5 CT images and thin section showing the traces of dissolution along the bedding planes. (a) 2D slices; (b) extraction of pores; (c) 3D reconstruction of pore networks, noting bedding plane with traces of dissolution; (d) aligned dissolution under microscopic observation.

distributed along the bedding planes (Figs. 6(b) and 6(c)). Additionally, two sets of aligned dissolution pore are observed along the bedding interfaces by thin section analysis (Fig. 6(d)). The framework grains (mainly quartz) are directionally aligned (Fig. 6(d)). Conversely, there are no evident bedding planes detected by the 2D CT slices (Fig. 7(a)), and consequently no obvious aligned dissolution pores (only slight signs of dissolution along the bedding planes) are detected by the 3D reconstruction of pore networks (Figs. 7(b)–7(c)). In addition, the dissolution pores only show weakly aligned under microscopic observation, and are very discontinuously distributed (Fig. 7(d)).

Thin sections confirm that the dissolution pores along bedding planes are mainly associated with the fine to medium grained sandstones which are abundant in feldspar and rock fragments (Figs. 5(d), 6(d), and 7(d)). Therefore both the CT images and thin section photomicrographs confirm that the effects of sedimentary beddings on improving framework grain dissolution. The presence of bedding planes will behave as flow pathways of acid-rich fluids, and therefore result in the formation of secondary dissolution porosity (Momeni et al., 2019).

5.2 NMR responses of dissolution pores

The reservoir spaces in sandstones include nanoscale (intercrystalline pores within authigenic clay minerals), microscale (micropores, intragranular dissolution pores), millimeter scale (large intergranular pores and moldic pores) (Lai et al., 2018, 2020). The dissolution of framework grains can form microscale or even millimeter scale pores along the bedding planes (Figs. 5–7). NMR test is commonly used to infer pore size distribution (Coates et al., 1991; Daigle et al., 2017). The presences of large dissolution pores along bedding planes (200–300 μm) or

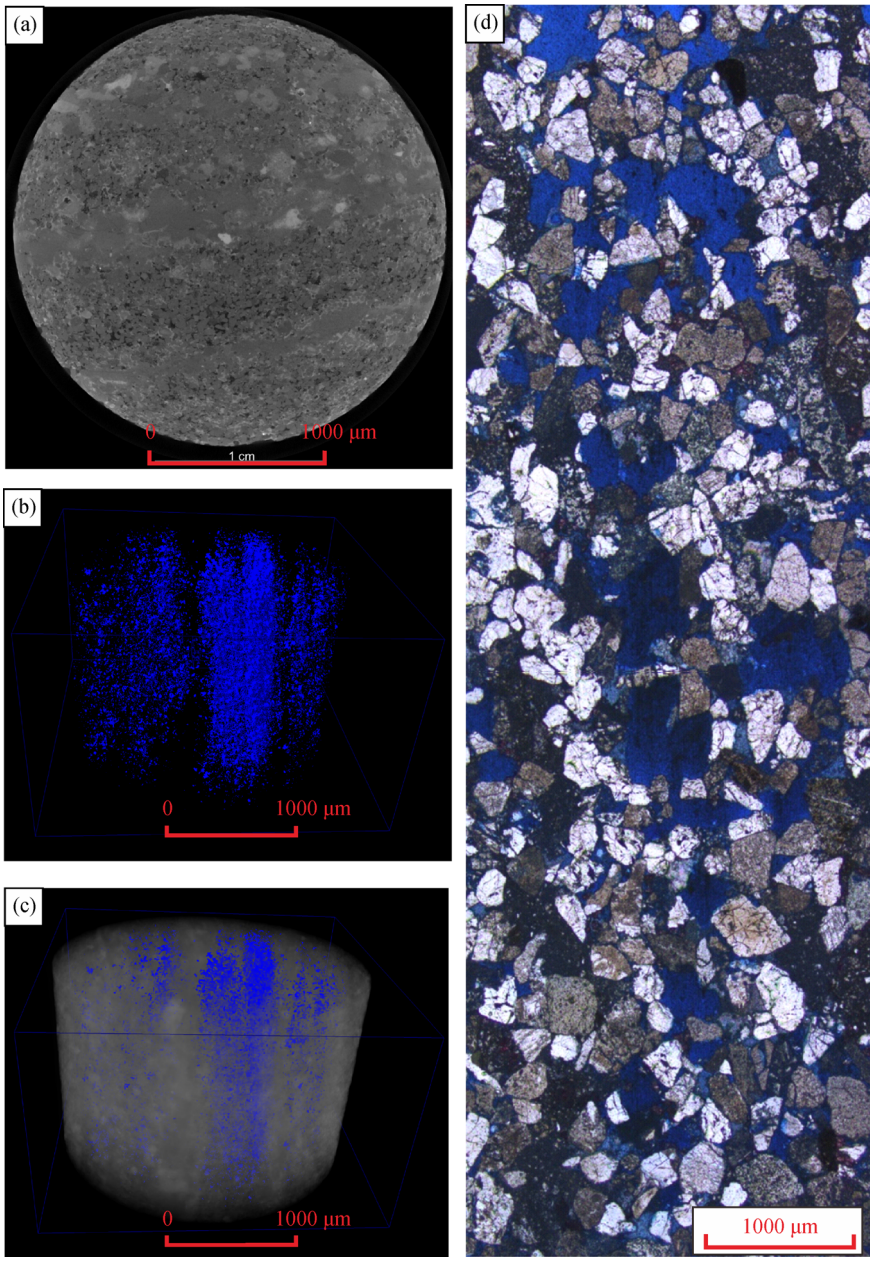

Fig. 6 CT images and related thin sections showing the bedding plane traced dissolution. (a) 2D slices; (b) extraction of pores; (c) 3D reconstruction of pore networks; (d) aligned dissolution pores.

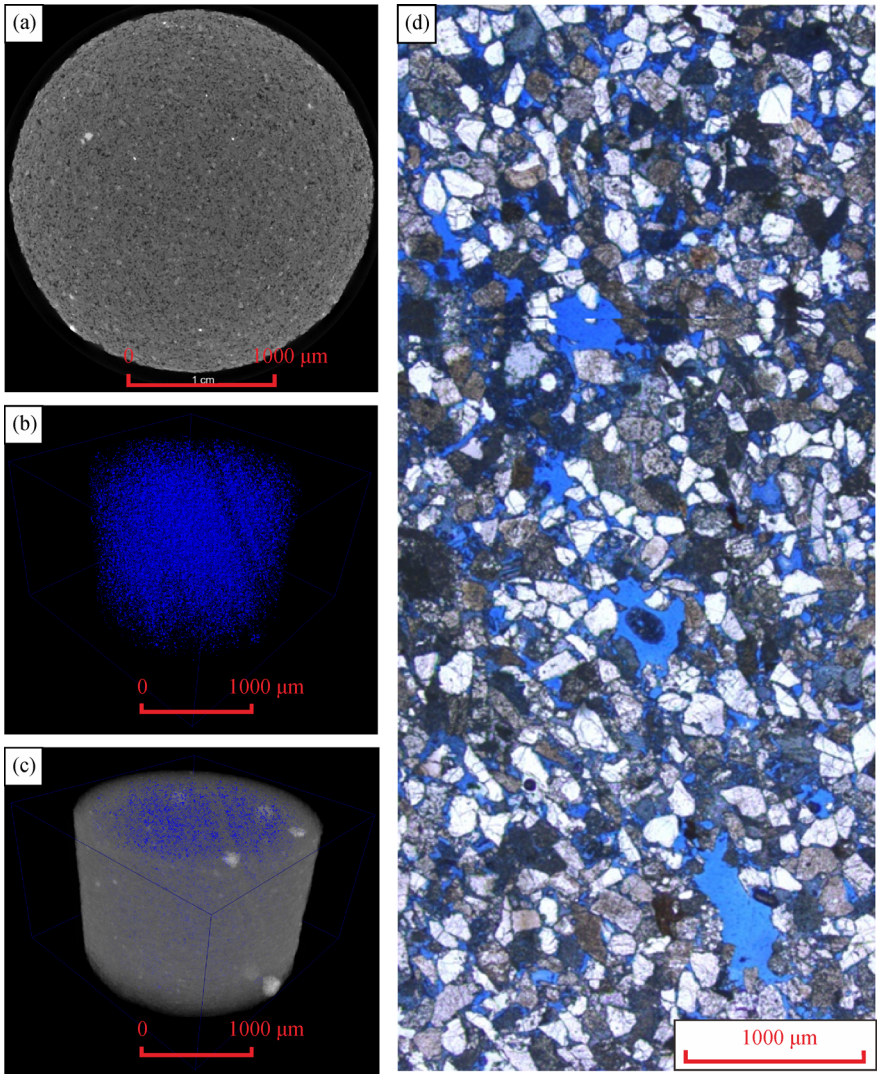

Fig. 7 Dissolution along the bedding planes recognized by CT images and thin sections. (a) 2D slices; (b) extraction of pores; (c) 3D reconstruction of pore networks; (d) weakly aligned dissolution.

intergranular pores refer to the large T_2 components (>100 ms), which relate to the right peak of a bimodal T_2 distribution ((Dillinger and Esteban, 2014) (Fig. 8(a)). Conversely, the micropores are associated with short T_2 components (left peak of the T_2 spectrum) (Rezaee et al., 2012; Daigle et al., 2014; Lai et al., 2016). The bi-modal T_2 behavior indicates the coexistence of micropores and large intergranular pores or even moldic pores (Fig. 8(a)), which is also evidenced by thin section observations (Fig. 8(b)), additionally the SEM image further confirms the presences of dissolution pores (Fig. 8(c)). The T_2 spectra at the saturated and centrifugal status in Fig. 8 are not evidently deviated, which implies that abundant pore systems are immovable, and actually the irreducible water content determined from the NMR test is as high as 62.45%, which is attributed to abundance of dissolution pores (Fig. 8). Therefore, the secondary dissolution pores are not always connected by effective pore throats (Dutton and Loucks, 2010; Lai et al., 2017), and a high irreducible water content from NMR tests will be encountered (Fig. 8).

6 Conclusions

The moldic pores, remnants in dissolution pores, and clay minerals within feldspar-hosted dissolution pores indicate that the sandstones are heavily dissolved. Bedding planes in fine-medium grained sandstones with high feldspar content are frequently enlarged by dissolution, while in the very fine-grained sandstones or clay rich sandstones, no bedding dissolution is observed. The diagenetic dissolution processes parallel to bedding planes varied greatly from that vertical to bedding planes. Layer structures (bedding planes) help improve the bedding-enhanced dissolution.

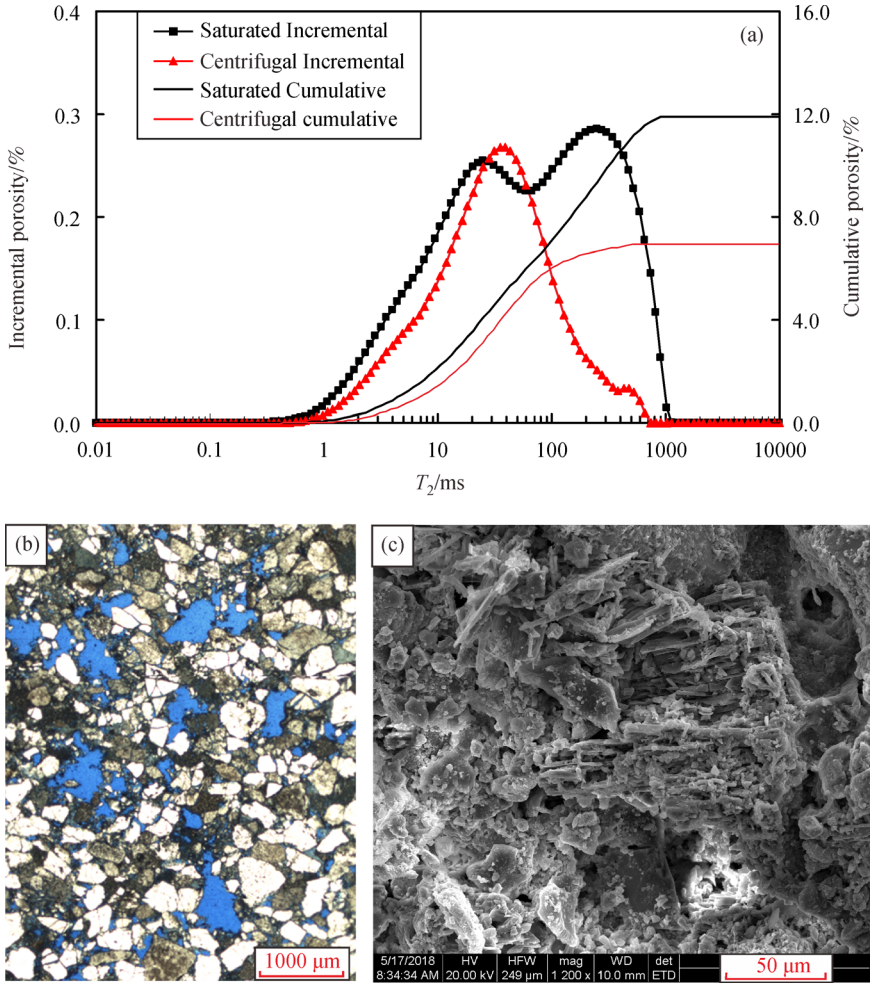

Fig. 8 NMR T_2 spectrum, SEM and thin section images showing the traces of dissolution along the bedding planes.(a) NMR T_2 spectrum; (b) thin sections showing the weakly aligned pores; (c) SEM image showing the feldspar dissolution pores.

Acknowledgements The PetroChina Jidong Oilfield Company is greatly acknowledged for providing samples and data access. This work is financially supported by Natural Science Foundation of Beijing (No. 8204069) and Science Foundation of China University of Petroleum, Beijing (No. 2462021YXZZ003).

References

Ajdukiewicz J M, Lander R H (2010). Sandstone reservoir quality prediction: the state of the art. AAPG Bull, 94(8): 1083–1091

Al-Ramadan K, Morad S, Proust J N, Al-Aasm I (2005). Distribution of diagenetic alterations in siliciclastic shoreface deposits within a sequence stratigraphic framework: evidence from the upper Jurassic, Boulonnais, NW France. J Sediment Res, 75(5): 943–959

Anders M H, Laubach S E, Scholz C H (2014). Microfractures: a review. J Structural Geo, 69 (Part B): 377–394

Bathurst R G C (1987). Diagenetically enhanced bedding in argillaceous platform limestones: stratified cementation and selective compaction. Sedimentology, 34(5): 749–778

Bjørlykke K, Jahren J (2012). Open or closed geochemical systems during diagenesis in sedimentary basins: constraints on mass transfer during diagenesis and the prediction of porosity in sandstone and carbonate reservoirs. AAPG Bull, 96(12): 2193–2214

Bjørlykke K (2014). Relationships between depositional environments, burial history and rock properties. Some principal aspects of diagenetic process in sedimentary basins. Sediment Geo, 301: 1–14

Bloch S, Lander R H, Bonnell L (2002). Anomalously high porosity and permeability in deeply buried sandstone reservoirs: origin and predictability. AAPG Bull, 86(2): 301–328

Bowen B B, Ochoa R I, Wilkens N D, Brophy J, Lovell T R, Fischietto N, Medina C R, Rupp J A (2011). Depositional and diagenetic variability within the Cambrian Mount Simon Sandstone: implications for carbon dioxide sequestration. Environ Geosci, 18(2): 69–89

Chang X, Shan Y F, Zhang Z H, Tang C A, Ru Z L (2015). Behavior of propagating fracture at bedding interface in layered rocks. Eng Geol, 197: 33–41

Chen X F, Li S M, Dong Y X, Pang X Q, Wang Z J, Ren M S, Zhang H C (2016). Characteristics and genetic mechanisms of offshore natural gas in the Nanpu Sag, Bohai Bay Basin, eastern China. Org Geochem, 94: 68–82

Chen L, Ji H C, Zhang L, Jia H B, Zhu Y, Fang Z (2017). Effect of burial

processes on the evolution of organic acids and implications for acidic dissolution from a case study of the Nanpu Sag, Bohai Bay Basin, China. J Nat Gas Sci Eng, 39: 173–187

Cnudde V, Boone M N (2013). High-resolution X-ray computed tomography in geosciences: a review of the current technology and applications. Earth Sci Rev, 123: 1–17

Coates G R, Peveraro R C A, Hardwick A, Roberts D (1991). The magnetic resonance imaging log characterized by comparison with petrophysical properties and laboratory core data. In: Proceedings of the 66th Annual Technical Conference and Exhibition. Formation Evaluation and Reservoir Geology, SPE 22723: 627–635

Daigle H, Thomas B, Rowe H, Nieto M (2014). Nuclear magnetic resonance characterization of shallow marine sediments from the Nankai Trough, Integrated Ocean Drilling Program Expedition 333. J Geophys Res, 119(4): 2631–2650

Daigle H, Hayman N W, Kelly E D, Milliken K L, Jiang H (2017). Fracture capture of organic pores in shales. Geophys Res Lett, 44(5): 2167–2176

Dashti R, Rahimpour-Bonab H, Zeinali M (2018). Fracture and mechanical stratigraphy in naturally fractured carbonate reservoirs—a case study from Zagros region. Mar Pet Geol, 97: 466–479

de Segonzac G D (1968). The birth and development of the concept of diagenesis (1866–1966). Earth Sci Rev, 4: 153–201

de Silva G P D, Ranjith P G, Perera M S A, Chen B (2016). Effect of bedding planes, their orientation and clay depositions on effective re-injection of produced brine into clay rich deep sandstone formations: implications for deep earth energy extraction. Appl Energy, 161: 24–40

Dillinger A, Esteban L (2014). Experimental evaluation of reservoir quality in Mesozoic formations of the Perth Basin (Western Australia) by using a laboratory low field Nuclear Magnetic Resonance. Mar Pet Geol, 57: 455–469

Dong Y X, Xiao L, Zhou H M, Wang C Z, Zheng J P, Zhang N, Xia W, Ma Q, Du J, Zhao Z, Huang H (2010). The tertiary evolution of the prolific Nanpu Sag of Bohai Bay Basin, China: constraints from volcanic records and tectono-stratigraphic sequences. Geol Soc Am Bull, 122(3–4): 609–626

Dong Y X, Zhao Z X, Wang J W, Du J X, Meng L J, Diao F (2015). Sequence stratigraphic patterns and sand body prediction models of fault-depressed lacustrine basins: a case study from the Dongying Formation in the Nanpu Sag, Bohai Bay Basin. Oil & Gas Geo, 36 (1): 96–102 (in Chinese)

Dutton S P, Loucks R G (2010). Diagenetic controls on evolution of porosity and permeability in lower Tertiary Wilcox sandstones from shallow to ultradeep (200–6700 m) burial, Gulf of Mexico Basin, USA. Mar Pet Geol, 27(1): 69–81

Flewelling S A, Tymchak M P, Warpinski N (2013). Hydraulic fracture height limits and fault interactions in tight oil and gas formations. Geophys Res Lett, 40(14): 3602–3606

Feng J L, Cao J, Hu K, Peng X Q, Chen Y, Wang Y F, Wang M (2013). Dissolution and its impacts on reservoir formation in moderately to deeply buried strata of mixed siliciclastic-carbonate sediments, northwestern Qaidam Basin, northwest China. Mar Pet Geol, 39(1): 124–137

Garzanti E (2019). Petrographic classification of sand and sandstone. Earth Sci Rev, 192: 545–563

Guan H, Zhu X M (2008). Sequence framework and sedimentary facies of Ed Formation in Paleogene, Nanpu Sag, Bohai Bay Basin. Acta Sediment Sin, 26(5): 730–736

Guo Y C, Pang X Q, Dong Y X, Jiang Z X, Chen D X, Jiang F J (2013). Hydrocarbon generation and migration in the Nanpu Sag, Bohai Bay Basin, Eastern China: insight from basin and petroleum system modeling. J Asian Earth Sci, 77(21): 140–150

Guo J G, Xu J, Guo F T, Li J H, Pang X Q, Dong Y X, Hu T (2016). Functional-element constraint hydrocarbon distribution model and its application in the 3rd member of Dongying Formation, Nanpu Sag, Bohai Bay Basin, Eastern China. J Petrol Sci Eng, 139: 71–84

Henares S, Caracciolo L, Viseras C, Fernandez J, Yeste L M (2016). Diagenetic constraints on heterogeneous reservoir quality assessment: a Triassic outcrop analog of meandering fluvial reservoirs. AAPG Bull, 100(9): 1377–1398

Higgs K E, Zwingmann H, Reyes A G, Funnell R H (2007). Diagenesis, porosity evolution, and petroleum emplacement in tight gas reservoirs, Taranaki Basin, New Zealand. J Sediment Res, 77(12): 1003–1025

Huang H X, Sun W, Ji W M, Chen L, Jiang Z X, Bai Y Y, Tang X L, Du K, Qu Y Q, Ouyang S Q (2018). Impact of laminae on gas storage capacity: a case study in Shanxi Formation, Xiasiwan Area, Ordos Basin, China. J Nat Gas Sci Eng, 60: 92–102

Islam M A (2009). Diagenesis and reservoir quality of Bhuban sandstones (Neogene), Titas Gas Field, Bengal Basin, Bangladesh. J Asian Earth Sci, 35(1): 89–100

Jafari J, Mahboubi A, Moussavi-Harami R, Al-Aasm I S (2020). The effects of diagenesis on the petrophysical and geochemicalattributes of the Asmari Formation, Marun oil feld, southwest Iran. Petrol Sci, 17(2): 292–316

Jiang F J, Pang X Q, Bai J, Zhou X H, Li J P, Guo Y H (2016). Comprehensive assessment of source rocks in the Bohai Sea area, Eastern China. AAPG Bull, 100(6): 969–1002

Lai J, Wang G W, Ran Y, Zhou Z L (2015). Predictive distribution of high quality reservoirs of tight gas sandstones by linking diagenesis to depositional facies: evidences from Xu-2 sandstones in Penglai area of central Sichuan Basin, China. J Nat Gas Sci Eng, 23: 97–111

Lai J, Wang G W, Fan Z Y, Chen J, Wang S C, Zhou Z L, Fan X Q (2016). Insight into the pore structure of tight sandstones using NMR and HPMI measurements. Energy Fuels, 30(12): 10200–10214

Lai J, Wang G W, Chai Y, Xin Y, Wu Q K, Zhang X T, Sun Y H (2017). Deep burial diagenesis and reservoir quality evolution of high-temperature, high-pressure sandstones: examples from Lower Cretaceous Bashijiqike Formation in Keshen area, Kuqa depression, Tarim basin of China. AAPG Bull, 101(6): 829–862

Lai J, Wang G W, Pang X J, Fan X C, Zhou Z L, Si Z W, Xie W B, Qin Z Q (2018). Effect of pore structure on reservoir quality and oiliness in Paleogene Dongying Formation sandstones in Nanpu Sag, Bohai Bay Basin, eastern China. Energy Fuels, 32(9): 9220–9232

Lai J, Pang X J, Xu F, Wang G W, Fan X C, Xie W B, Chen J Y, Qin Z Q, Zhou Z L (2019). Origin and formation mechanisms of low oil saturation reservoirs in Nanpu Sag, Bohai Bay Basin, China. Mar Pet Geol, 110: 317–334

Lai J, Fan X C, Liu B C, Pang X J, Zhu S F, Xie W B, Wang G W (2020). Qualitative and quantitative prediction of diagenetic facies via well

logs. Mar Pet Geol, 120: 104486

Lai J, Liu S, Xin Y, Wang S, Xiao C, Song Q, Chen X, Wang G, Qin Z, Ding X (2021). Geological-petrophysical insights in the deep Cambrian dolostone reservoirs in Tarim Basin, China. AAPG Bull, 105(11): 2263–2296

Lee H P, Olson J E, Holder J, Gale J F W, Myers R D (2015). The interaction of propagating opening mode fractures with preexisting discontinuities in shale. J Geophys Res Solid Earth, 120(1): 169–181

Liang C, Cao Y C, Liu K Y, Jiang Z X, Wu J, Hao F (2018). Diagenetic variation at the lamina scale in lacustrine organic-rich shales: implications for hydrocarbon migration and accumulation. Geochim Cosmochim Acta, 229: 112–128

Liu D D, Li Z, Jiang Z X, Zhang C, Zhang Z Y, Wang J B, Yang D X, Song Y, Luo Q (2019). Impact of laminae on pore structures of lacustrine shales in the southern Songliao Basin, NE China. J Asian Earth Sci, 182: 103935

Liu M J, Liu Z, Wang B, Sun X M, Guo J G (2015). A new method for recovering paleoporosity of sandstone: case study of middle E_{s3} member of Paleogene formation in Niuzhuang Sag, Dongying Depression, Bohai Bay Basin in China. Front Earth Sci, 9(3): 521–530

Liu L, Chen H D, Zhong Y J, Wang J, Xu C G, Chen A Q, Du X F (2017). Sedimentological characteristics and depositional processes of sediment gravity flows in rift basins: the Palaeogene Dongying and Shahejie Formations, Bohai Bay Basin, China. J Asian Earth Sci, 147: 60–78

Momeni A, Rostami S, Hashemi S, Mosalman-Nejad H, Ahmadi A (2019). Fracture and fluid flow paths analysis of an offshore carbonate reservoir using oil-based mud images and petrophysical logs. Mar Pet Geol, 109: 349–360

Morad S, Al-Ramadan K, Ketzer J M, DeRos L F (2010). The impact of diagenesis on the heterogeneity of sandstone reservoirs: a review of the role of depositional facies and sequence stratigraphy. AAPG Bull, 94(8): 1267–1309

Niu H P, Liu S C, Lai J, Wang G W, Liu B C, Xie Y Q, Xie W B (2020). *In situ* stress determination and fracture characterization using image logs. Energy Sci Eng, 8(2): 476–489

Rezaee R, Saeedi A, Clennell B (2012). Tight gas sands permeability estimation from mercury injection capillary pressure and nuclear magnetic resonance data. J Petrol Sci Eng, 88–89: 92–99

Rossi C, Marfil R, Ramseyer K, Permanyer A (2001). Facies-related diagenesis and multiphase siderite cementation and dissolution in the reservoir sandstones of the Khatatba Formation, Egypt's Western Desert. J Sediment Res, 71(3): 459–472

Saïag J, Brigaud B, Portier É, Desaubliaux G, Bucherie A, Miska S, Pagel M (2016). Sedimentological control on the diagenesis and reservoir quality of tidal sandstones of the Upper Cape Hay Formation (Permian, Bonaparte Basin, Australia). Mar Pet Geol, 77: 597–624

Schmid S, Worden R H, Fisher Q J (2004). Diagenesis and reservoir quality of the Sherwood Sandstone (Triassic), Corrib Field, Slyne Basin, west of Ireland. Mar Pet Geol, 21(3): 299–315

Stonecipher S, Winn J R, Bishop M (1984). Diagenesis of the frontier formation, Moxa Arch: a function of sandstone geometry, texture and composition, and fluid flux. AAPG Bull, 68: 289–316

Swanson S K (2007). Lithostratigraphic controls on bedding-plane fractures and the potential for discrete groundwater flow through a siliciclastic sandstone aquifer, southern Wisconsin. Sediment Geol, 197(1–2): 65–78

Tang J Z, Wu K, Zeng B, Huang H Y, Hu X D, Guo X Y, Zuo L H (2018). Investigate effects of weak bedding interfaces on fracture geometry in unconventional reservoirs. J Petrol Sci Eng, 165: 992–1009

Taylor T R, Giles M R, Hathon L A, Diggs T N, Braunsdorf N R, Birbiglia G V, Kittridge M G, Macaulay C I, Espejo I S (2010). Sandstone diagenesis and reservoir quality prediction: models, myths, and reality. AAPG Bull, 94(8): 1093–1132

Tucker M E (2003). Sedimentary Rocks in the Field (3rd ed). Chichester: John Wiley & Sons

Wang J K, Fu Y X, Yan Z X, Fu J L, Xie J, Li K K, Zhao Y F (2021). Influence of sedimentation and diagenesis on reservoir physical properties: a case study of the Funing Formation, Subei Basin, eastern China. Front Earth Sci, 15(4): 892–908

Wang G W, Lai J, Liu B C, Fan Z Y, Liu S C, Shi Y J, Zhang H T, Chen J (2020). Fluid property discrimination in dolostone reservoirs using well logs. Acta Geol Sin, 94(3): 831–846

Weng X W, Chuprakov D, Kresse O, Prioul R, Wang H T (2018). Hydraulic fracture-height containment by permeable weak bedding interfaces. Geophysics, 83(3): MR137–152

Worthington S R H, Davies G J, Alexander E C Jr (2016). Enhancement of bedrock permeability by weathering. Earth Sci Rev, 160: 188–202

Xu A N, Zheng H J, Dong Y X, Wang Z C, Yin J F, Yan W P (2006). Sequence stratigraphic framework and sedimentary facies prediction in Dongying Formation of Nanpu Sag. Pet Explor Dev, 33(4): 437–443

Xu C, Gehenn J M, Zhao D, Xie G, Teng M K (2015). The fluvial and lacustrine sedimentary systems and stratigraphic correlation in the Upper Triassic Xujiahe Formation in Sichuan Basin, China. AAPG Bull, 99(11): 2023–2041

Yandoka B M S, Abubakar M B, Abdullah W H, Maigari A S, Hakimi M H, Adegoke A K, Shirputda J J, Aliyu A (2015). Sedimentology, geochemistry and paleoenvironmental reconstruction of the Cretaceous Yolde formation from Yola Sub-basin, Northern Benue Trough, NE Nigeria. Mar Pet Geol, 67: 663–677

Yue D L, Wu S H, Xu Z Y, Xiong L, Chen D X, Ji Y L, Zhou Y (2018). Reservoir quality, natural fractures, and gas productivity of Upper Triassic Xujiahe tight gas sandstones in western Sichuan Basin, China. Mar Pet Geol, 89: 370–386

Zazoun R S (2013). Fracture density estimation from core and conventional well logs data using artificial neural networks: the Cambro-Ordovician reservoir of Mesdar Oil Field, Algeria. J Afr Earth Sci, 83: 55–73

Zeng L B, Li X Y (2009). Fractures in sandstone reservoirs with ultra-low permeability: a case study of the Upper Triassic Yanchang Formation in the Ordos Basin, China. AAPG Bull, 93(4): 461–477

Zhang J G, Jiang Z X, Gierlowski-Kordesch E, Xian B Z, Li Z P, Wang S Q, Wang X B (2017). A double-cycle lake basin formed in extensional to transtensional setting: the Paleogene Nanpu sag, Bohai Bay Basin, China. Sediment Geo, 349: 15–32

Zhang G Y, Wang Z Z, Guo X G, Sun Y N, Sun L, Pan L (2019).

Characteristics of lacustrine dolomitic rock reservoir and accumulation of tight oil in the Permian Fengcheng Formation, the western slope of the Mahu Sag, Junggar Basin, NW China. J Asian Earth Sci, 178: 64–80

Zhang R H, Wang K, Zeng Q L, Yu C F, Wang J P (2021). Effectiveness and petroleum geological significance of tectonic fractures in the ultra-deep zone of the Kuqa foreland thrust belt: a case study of the Cretaceous Bashijiqike Formation in the Keshen Gasfield. Petrol Sci, 18: 728–741

Zhang K X, Lai J, Bai G P, Pang X J, Ma X Q, Qin Z Q, Zhang X S, Fan X C (2020). Comparison of fractal models using NMR and CT analysis in low permeability sandstones. Mar Pet Geol, 112: 104069

Zhou J, He S M, Tang M, Huang Z, Chen Y L, Chi J, Zhu Y, Yuan P (2018). Analysis of wellbore stability considering the effects of bedding planes and anisotropic seepage during drilling horizontal wells in the laminated formation. J Petrol Sci Eng, 170: 507–524